



Channel utilization of media access control protocols for underwater acoustic networks with propagation delay and mobility^{a)}

Ruoyu Wangb) and Y. Rosa Zheng

Department of Electrical and Computer Engineering, Lehigh University, Bethlehem, Pennsylvania 18015, USA

ABSTRACT:

This paper investigates the impact of mobility on underwater acoustic communication networks in which the propagation delay is comparable to or larger than the packet duration. An underwater acoustic wireless network, consisting of static and mobile nodes, is studied for its link-layer channel utilization. Synchronous and asynchronous media access control (MAC) protocols are employed with ALOHA, TDMA (time-division multiple access), and artificial intelligence (AI) agent nodes. The simulation results of a multi-node network show that the asynchronous MAC protocols achieve up to 6.66× higher channel utilization than synchronous protocols by allowing time slots to be shorter than the maximum propagation delay among nodes and permitting asynchronous transmission time. The high mobility of a few mobile nodes also favors asynchronous protocols and increases the overall channel utilization. However, node mobility causes more difficulties for the AI node to learn the environment, which may be ineffective to achieve higher gains in channel utilization. © 2024 Acoustical Society of America.

https://doi.org/10.1121/10.0026232

(Received 12 October 2023; revised 3 May 2024; accepted 20 May 2024; published online 12 June 2024)

[Editor: Aijun Song] Pages: 3782-3793

I. INTRODUCTION

Internet of underwater things (IoUT) has found important applications in the blue economy such as ocean exploration, seafloor mapping, deep sea mining, underwater environment and infrastructure monitoring, offshore oil and gas, and offshore fishery and aquaculture. To transfer data from IoUT nodes to the internet, most IoUT networks use cabled communication systems because of unreliable underwater wireless communication. However, cable and cable management are problematic for mobile underwater nodes, such as Argos (Shepard et al., 2012), gliders (Lee et al., 2011), underwater mobile robots (Assaf et al., 2013; Williamson et al., 2017), and autonomous underwater vehicles (AUVs). The fast growth in the IoUT sector also drives the tremendous demands on reliable and efficient underwater acoustic wireless networks (UANs) as acoustic propagation is the most effective means of medium-range underwater wireless communication (Stojanovic Preisig, 2009), whereas radio frequency (RF; Akyildiz et al., 2015) or optical means (Diamant et al., 2017) suffer from strong attenuation in water when the communication ranges are greater than 100 m.

However, UAN also suffers from tremendous difficulties due to its limited bandwidth, large propagation delays, and lack of infrastructure support (Akyildiz et al., 2005; Zheng et al., 2015). As a result of frequency-related attenuation, UAN has a limited bandwidth on the order of 10 kHz (Stojanovic and Preisig, 2009), rather than megahertz or gigahertz, which are available in the RF networks. Therefore, spectrum sharing becomes difficult, and the time duration of a UAN packet is often quite long. The nominal sound speed in water is 1500 m/s, which causes large propagation delays that are comparable to or longer than the packet duration (Chitre et al., 2014; Chitre and Soh, 2015). The mobility of IoUT nodes also affects the packet arrival time, which leads to significant time variation. The lack of infrastructure support results in difficulties in timing alignment, location service, or resource allocation among network nodes. These difficulties bring formidable challenges to UANs (Al Guqhaiman et al., 2021; Jiang, 2017), resulting in small channel capacity, low reliability, and low network efficiency (Lmai et al., 2017; Zeng et al., 2017).

The unique environment in UANs calls for innovative media access control (MAC) protocols as the direct application of RF MAC protocols in UANs would result in low efficiencies (Al Guqhaiman et al., 2021; Geng and Zheng, 2022). Not only MAC protocols but MAC design strategies, which were initially developed for RFs, may be ineffective in UANs (Jiang, 2017). For example, carrier sensing multiple access with collision avoidance (CSMA/CA) is widely used in RF networks such as WiFi. The underlying assumption is that the nodes in the network can hear the carrier being used instantly, hence, they would avoid transmitting at the same time. However, when applied in underwater acoustic sensor networks (Fang et al., 2010), CSMA/CA

a)Portions of this work have been presented in "Exploring propagation delay and mobility in underwater acoustic networks," in 184th Meeting of the Acoustical Society of America, Chicago, IL, 8-12 May 2023.

b)Email: ruw220@lehigh.edu

yields low channel utilization (Al Guqhaiman et al., 2021; Han and Fei, 2016; Hwang and Cho, 2016) because the large propagation delays require the nodes to hear for long periods to avoid potential collisions or sophisticated handshaking, and location tracking may be required to improve the efficiency (Nguyen et al., 2007). Another example is timedivision multiple access (TDMA), which is widely used in cellular networks, and its time-spectrum efficiency is as high as 85% because a central resource scheduler assigns multiple nodes to tightly-fit subslots within a time slot. However, when applied to UAN, it is difficult to align the time of arrivals from multiple nodes into a tight time slot because of the large variations in propagation delays. As a result, each node should be assigned an entire time slot, and multiple nodes are scheduled to transmit packets in a roundrobin fashion, leading to low channel utilization. Special timing arrangement can be achieved when the nodes are placed in a special pattern in the space (Lmai et al., 2017), thus, achieving higher throughput. Other variations of TDMA-based UAN protocols (Kredo et al., 2009; Morozs et al., 2018) also exploit the propagation delays in the network to facilitate TDMA in UAN.

Most existing underwater MACs are designed for static networks, assuming nodes are fixed in space and can obtain instant feedback. However, node mobility leads to further timing variations and more severe Doppler effects, making it harder to design MACs. The challenges in analyzing mobile UANs exist in three aspects. First, the mobility models of underwater environments are complex, involving ocean currents, tides, and motion of communication platforms. The detailed modeling often requires high computational complexity, but the impact of mobility on the communication links can be greatly simplified. Second, node mobility introduces additional variations in propagation delays, which have diverse impacts on different MAC protocols. For example, time variations require that the system clock be re-synchronized in centralized schedule-based MACs or the waiting time be redefined in handshakingbased MACs. Also, mobility induces the Doppler effects, which distorts the decision margin in the physical layer, resulting in increased bit error rate (BER) and packet losses. The poor performance in the physical layer means more retransmissions and lower network efficiency (Akyildiz et al., 2005). Third, the interaction between node mobility and emerging MAC protocols that involve artificial intelligence (AI) nodes are largely unexplored. Field experimental data are hardly available for AI training. Simulators are mostly event-based without accurate tracking of timing in the network. Therefore, simulators need to be redesigned to generate training data for AI nodes.

This paper analyzes the channel utilization of different underwater acoustic MAC protocols with a single-hop star topology in which multiple source nodes transmit to a single sink node. Several simulation experiments are designed to investigate the impact of node mobility on static or mobile networks with synchronous or asynchronous MAC protocols and with or without AI nodes. To extend the capacity of

link-layer simulation, we improved the time-based simulator in Geng and Zheng (2022) and designed a new lightweight simulator that incorporates the mobility models into the MAC protocols. The simulation results show that node initial locations have strong impacts on channel utilization in static networks with synchronous MAC protocols, but node mobility helps to reduce packet collisions caused by bad initial location settings in synchronous protocols. High mobility also increases channel utilization in asynchronous protocols similar to the effect of an AI node. However, high mobility causes more difficulties for the AI node to learn the environment, thus, the combination of node mobility and AI node may not achieve more gains in channel utilization.

II. RELATED WORKS

MAC protocols are usually classified into contentionfree and contention-based protocols (Al Guqhaiman et al., 2021). The contention-free protocols refer to schedule-based protocols, where a scheduler allocates the frequency, time, or code resources to multiple nodes to share the communication medium. In underwater scenarios, schedule-based protocols, such as TDMA, frequency division multiple access (FDMA), or code division multiple access (CDMA), are widely explored. For example, Pompili et al. (2007) explored UAN CDMA. Alfouzan et al. (2019) proposed the graph coloring-MAC, which is a TDMA-based MAC. Nguyen et al. (2007) investigated FDMA and concluded that FDMA is unsuitable for UANs because of the limited bandwidth. These conventional schedule-based protocols, originally developed for RF networks, suffer from inefficiency in UAN as a result of the long propagation delay, huge multipath, Doppler effects, and limited bandwidth. To overcome the shortcomings in schedule-based protocols, many modifications have been proposed. For example, transmit delay allocation-MAC (Morozs et al., 2018) is based on TDMA without requiring clock synchronization. Underwater distributed-TDMA (Li et al., 2009) is a distributed TDMA MAC protocol without requiring a central scheduler. Nevertheless, contention-free MAC protocols require significant underwater infrastructure, such as base stations and backbone networks, to be effective.

Contention-based protocols share communication resources on demand in contrast to fixed scheduling. The contention-based MAC protocols are classified into handshaking-based, random access, and learning-based protocols. Handshaking-based protocols, such as M-FAMA (Han et al., 2013), DACAP (Peleato and Stojanovic, 2007), and CUMAC-CAM (Rahman et al., 2019), are suitable for networks with high data rates, large packet sizes, and short transmission ranges. However, the transmission of handshaking messages, such as request to send (RTS) and clear to send (CTS), occupies limited bandwidth and introduces large delays in long-distance networks (Han et al., 2013). Random access MACs include CSMA-based protocols and ALOHA-based protocols. The CSMA-based random access protocols, such CSMA/CA (Fang et al., 2010), suffer from

https://doi.org/10.1121/10.0026232

inefficient and inaccurate carrier sensing (Al Guqhaiman et al., 2021; Han and Fei, 2016; Hwang and Cho, 2016). ALOHA-based protocols, such as ALOHA-CA (Chirdchoo et al., 2007) and CW-ALOHA (Parrish et al., 2008), are suitable for networks with low data rates, small packet sizes, and long transmission ranges. Learning-based protocols introduce the intelligent node, called "agent," and use machine learning (ML) and historical observations in the channel to learn the environment and improve channel utilization without increasing collision rates. The learning-based protocols include async-DL-MAC (Geng and Zheng, 2022), UW-ALOHA-Q (Park et al., 2019), and ALOHA-QIR (Chu et al., 2012). Furthermore, the random access and learningbased MAC protocols are capable of concurrent transmission because these protocols can be asynchronous and distributed. By shortening the duration of a time slot, enabling transmission before arrival, and allowing the packets to arrive across different time slots (Chen et al., 2021; Geng and Zheng, 2022; Park et al., 2021; Sitanayah et al., 2010), concurrent transmission is effective in using long propagation delays in underwater channels and increasing channel utilization (Zhuo et al., 2022).

Limited work illustrates the capability of MAC protocols in UANs with mobility. DAP-MAC (Han and Fei, 2016) claims that the DAP-MAC can handle mobility well. M-FAMA (Han *et al.*, 2013) discusses the impacts of mobility and evaluates the MAC performance under the meandering current mobility (MCM). The UW-ALOHA-QM protocol (Park *et al.*, 2021) studies a few different mobility models and their effects on MAC protocols. This paper thoroughly investigates the impact of mobility on genetic MAC protocols, especially with learning-based MAC protocols.

Conventional network simulation tools have limited capabilities to simulate emerging network functions such as mobility, ML-agent, and hybrid MAC networks. Currently, network simulator 3 (NS-3; Riley and Henderson, 2010; UAN, 2024), UnetStack3 (Chitre et al., 2014), DESERT (Campagnaro et al., 2016), and SUNSET (Petrioli et al., 2015) are the commonly used simulators for UAN, and provide full protocol stack simulation. For example, the NS-3 UAN framework consists of propagation models, physical channel models, UAN MAC protocols, and AUV mobility models. The physical channel model of the NS-3 UAN framework consists of the packet error rate (PER) model and signal-to-noise ratio (SNR) model (UAN, 2024). NS-3 MAC module contains ALOHA, CW-ALOHA (Parrish et al., 2008), and RC-MAC (UAN, 2024) protocols. The ALOHA and CW-ALOHA use the default PER model, which tests the packet against a SNR threshold and assumes error with probability one if the SNR is below the threshold or success if the SNR is above the threshold. The AUV mobility models provide control and navigation models for several vehicle types and can simulate vehicle trajectories. These models may be used by MAC protocols to estimate the propagation delays in the link layer. However, NS-3 is an event-based simulator that is efficient in accelerating full-stack simulation but has inherent difficulties in tracking every time step accurately. This makes NS-3 difficult to simulate learning-based MAC protocols, such as async-DL-MAC (Geng and Zheng, 2022) and UW-ALOHA-QM (Park et al., 2021), because the AI node requires historical channel observation information to train the learning model dynamically. Unlike the full-stack simulation, this paper implements a lightweight, open-source link-layer simulator that focuses on link-layer simulation with time-based approaches. The lightweight simulator is capable of simulating static or mobile nodes, synchronous or asynchronous transmissions, and with or without an AI-agent node. NS-3 (Riley and Henderson, 2010; UAN, 2024) used some experiments that validate the simulation results.

III. MOBILE UAN MODELING

This paper discusses a single-hop star-topology underwater wireless sensor network. The sink node is assumed to be static at a fixed location while the N source nodes can be static or mobile. The system in this paper is a slotted network in which the time dimension is uniformly segmented into multiple time slots with length T. Because of hardware constraints and timing requirements, each source node experiences a setup delay, $T_r(n,t)$ for n = 1,...,N at the beginning of the tth time slot. After the setup delay, the source node emits modulated acoustic waveforms for T_p seconds, where T_p is the packet duration. The underwater space is modeled as a three-dimensional (3D) Cartesian coordinate system with the sink node located at the origin and the source nodes randomly distributed around the sink node within a sphere of radius $L_{\rm max}$. The propagation delay of the *n*th source node to the sink is denoted as τ_n for *n* = 1, 2, ..., N and is calculated by $\tau_n = L_n/V$, where L_n is the distance between the nth source node and the sink node, and V is the acoustic propagation speed.

Compared with RF networks, the prolonged propagation delay in acoustic communication leads to low channel utilization. Even if the RF networks and UANs choose the same bit rate $(T_{pRF} = T_{pUAN})$, the channel occupancy of the UAN is sparser than that for RF networks, as shown in Fig. 1, where the propagation delay in the RF networks is negligible, such that the source nodes can choose carrier sensing multiple access (CSMA) to reduce collision, and the length of a time slot is set to be comparable to the packet duration. If the slotted ALOHA protocol is used, the overall channel utilization of RF networks will approach 1/e, where e ≈ 2.71828 is Euler's number. In contrast, the large propagation delay in UAN requires that a time slot of synchronous protocols be longer than the maximum propagation delay of the network, which is much longer than the packet duration, resulting in sparse utilization of the channel. It is difficult for source nodes to sense the carriers of other transmissions because two nodes can be out of range of each other. Multiple source nodes can transmit in the same time slots, and collisions occur if signals from different source nodes arrive at the sink node at the same time. The overall channel utilization of the UAN is very low if conventional TDMA or slotted ALOHA protocols are applied directly in the UAN.

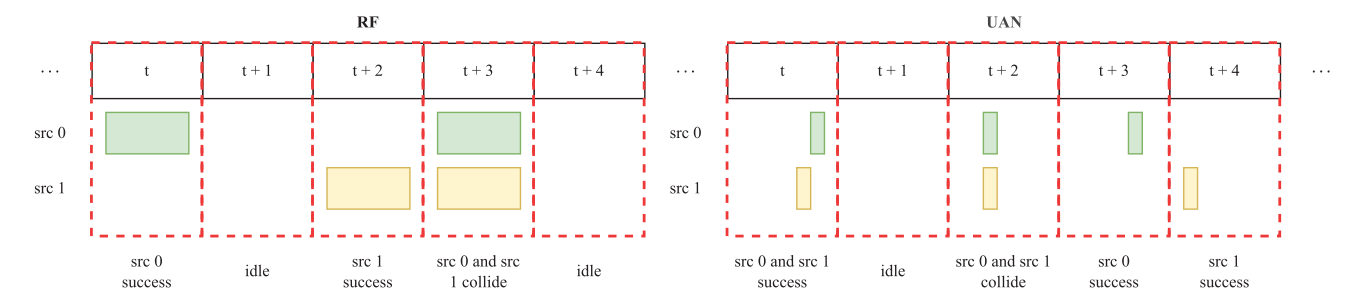


FIG. 1. (Color online) (Left) RF slotted network and (right) UAN slotted network are shown. Because of the long propagation delay, UANs use longer time slots, and the channel utilization is relatively lower than that for RF networks.

Although accurate clock synchronization is impractical to maintain in UANs, a synchronous MAC can still assume a coarse-grained globally synchronized clock for all nodes in the network, and different source nodes could transmit packets at almost the same time at the beginning of each time slot. This means that

$$T_r(1,t) = T_r(2,t) = \dots = T_r(N,t) \quad \forall t \in \mathbb{Z}, \tag{1}$$

where \mathbb{Z} denotes the set of integers. This paper assumes that $T_r(n,t) \equiv 0$, $\forall n \in [1,N] \cap \mathbb{Z}$, $\forall t \in \mathbb{Z}$ in synchronous networks. A guard time, $T_g \geq T_p$, is added at the end of the time slot to guarantee that a packet transmitted in the tth time slot is also received within the tth time slot. Therefore, the time slot length, T, of a synchronous network has to satisfy the following constraint:

$$T \ge \max\{T_r(1,t) + \tau_1, ..., T_r(n,t) + \tau_n, ..., T_r(N,t) + \tau_N\} + T_g.$$
(2)

Usually, the location of each source node is unknown to the network designer, and a long time slot, $T \geq \max(T_r(n,t)) + L_{\max}/V + T_g$, should be chosen to guarantee that the packet arrives within the time slot. For example, if $L_{\max} = 1500$ m, then the maximum propagation delay is $\tau_{\max} = 1500/1500 = 1$ s, which is often much larger than a packet duration, leading to very sparse occupancy of the communication channel.

Asynchronous MAC protocols enable concurrent transmission, which allows the transmission of a new packet before the arrival of the previous packet. Therefore, asynchronous nodes independently and randomly pick $T_r(n,t)$ to avoid potential collisions. The length of time slot in asynchronous networks can be selected to be shorter than $L_{\rm max}/V+T_g$ and T_g can be set to zero. With a shorter time slot, more packets are transmitted in a unit of time. Meanwhile, denser packet transmissions lead to higher collision probabilities. Figure 2 illustrates the timing models in the synchronous and asynchronous networks. Without loss of generality, we assume that the packet duration, T_p , is the same for all source nodes.

Once a packet arrives at the sink node, the sink node will be busy for a T_p period to fully receive the packet. We assume any other arrivals during this busy time will cause a *collision*. In synchronous networks, collision only happens

when source nodes located at similar distances from the sink node happen to transmit simultaneously. If a collision occurs between the *n*th and *m*th nodes, then

$$\tau_m - T_p \le \tau_n \le \tau_m + T_p$$

$$\Rightarrow L_m - T_p V \le L_n \le L_m + T_p V \quad \forall m, n \in \mathbb{Z} \cap [1, N].$$
(3)

In an asynchronous network, a packet arrives in the same or subsequent time slot of the transmitting slot. Assuming that $L_n \geq L_m$ and $\lfloor L_{\max}/(VT) \rfloor = K_{\max}$, the collision condition becomes

$$kT + \tau_m - T_p \le \tau_n \le kT + \tau_m + T_p$$

$$\forall m, n \in \mathbb{Z} \cap [1, N], \ \forall k \in \mathbb{Z} \cap [0, K_{\text{max}}]. \tag{4}$$

Channel utilization in an asynchronous network can be increased when the length of a time slot, T, is reduced while collisions are avoided as much as possible. Therefore, the selections of T and T_p and the locations of the source nodes are important in asynchronous network design.

To simulate the effect of mobile nodes in the network, the propagation delays of the mobile nodes are computed by assuming that the velocity of the mobile nodes stays unchanged within a time duration, Δt . If the nth node is mobile and its velocity at time, t_0 , is $\vec{v}_n(t_0)$, then the propagation delay, τ_n , in the mobile network becomes a function of t_0 as

$$\tau_n(t_0 + \Delta t) = \tau_n(t_0) + \vec{v}_n(t_0)\Delta t/V. \tag{5}$$

The propagation delays from the initial source locations to the sink node are iteratively computed throughout the simulation. The mobility comes from the underwater environment and communication platforms. The mobility from the environment is passive and caused by currents such as chaotic stirring (Beerens et al., 1994) and MCM (Caruso et al., 2008). Mobility from the communication platforms, such as that bounded to boats or AUVs, is active. This paper simulates passive and active mobility in an accumulative way such that $\overrightarrow{v_{\text{total}}} = \overrightarrow{v_{\text{passive}}} + \overrightarrow{v_{\text{active}}}$. For example, in an AUV-assisted sensor network (Park et al., 2021; Purcell et al., 2011), all source nodes are attached to AUVs that sense the environment and plan paths dynamically to finish their tasks such as searching for wreckage in a zig-zag path in a crash area (Purcell et al., 2011). Based on the MCM model (Caruso et al., 2008), the passive velocity is

https://doi.org/10.1121/10.0026232 JASA

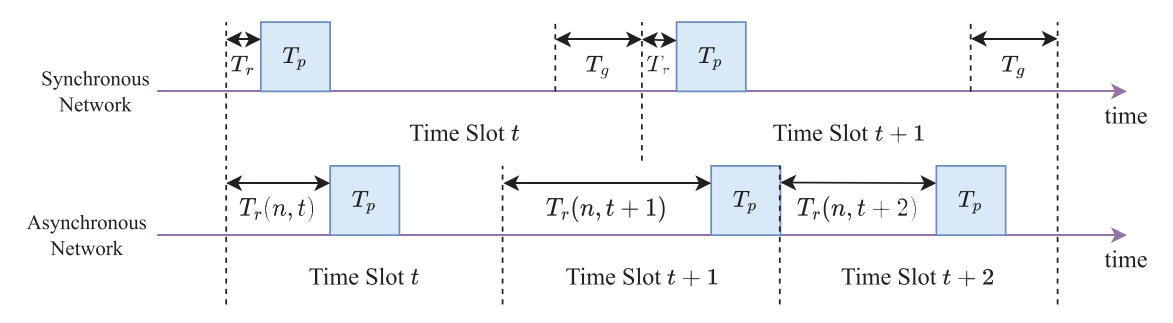


FIG. 2. (Color online) Time models for synchronous and asynchronous networks. Source nodes in a synchronous MAC transmit at the same starting time, $T_r(n,t)$, whereas nodes in an asynchronous network can pick arbitrary starting times, $T_r(n,t)$. A synchronous network has to use a longer time slot than the asynchronous network.

 $|\overline{v_{\mathrm{passive}}}| = \sqrt{v_x^2 + v_y^2} \le 0.3 \,\mathrm{m/s}$, and the mobilities for all nodes are strong correlated. Based on the parameters of the state-of-the-art AUVs, the active velocity rule is $|\overline{v_{\mathrm{active}}}| = \sqrt{v_x^2 + v_y^2 + v_z^2} \in [2,4] \,\mathrm{m/s}$, and the mobilities for all nodes are independent. In this AUV-assisted network, all nodes move with the dynamic velocity, $\overline{v_{\mathrm{total}}}$, and their propagation delays change correspondingly. Another example is the moored floating sensor network (Park *et al.*, 2021) in which all source nodes float on the ocean surface with a tether anchored at a fixed point. The mobility only comes from ocean currents within a limited range of motion. This model follows the velocity rule, $|\overline{v_{\mathrm{passive}}}| = \sqrt{v_x^2 + v_y^2} \le 0.3 \,\mathrm{m/s}$, and $|\overline{v_{\mathrm{active}}}| = 0$. Unlike the AUV-assisted network, the moored floating sensors are limited in their range of motion.

To simulate the mobility and its impact on MAC protocols, we design a lightweight, open-source link-layer simulator that employs three levels of abstraction to simulate the interaction between different types of source nodes and the sink node, as shown in Fig. 3. The ENVIRONMENT level determines whether the network status is a successful reception or packet collision and evaluates channel utilization and throughput performance. The CHANNEL level implements the network timing model, such as propagation delays, packet duration, mobility-induced delay variations, etc. The CHANNEL level uses a PER model, which is the same as NS-3's default PHY model (UAN, 2024). DELAY QUEUE level provides the time-accurate simulation of the propagation, computes the propagation delays in point-to-point communication links, and implements the transmission model with precise packet data and duration.

To achieve the fine granularity of time, the simulator divides a time slot further into multiple sub-slots to uniformly simulate synchronous and asynchronous timing models. The simulator discretizes T, T_p , T_r , and T_g into integer multiples of δ as

$$K = \left\lceil \frac{T}{\delta} \right\rceil, \quad k_p = \left\lceil \frac{T_p}{\delta} \right\rceil, \quad k_r = \left\lceil \frac{T_r}{\delta} \right\rceil, \quad k_g = \left\lceil \frac{T_g}{\delta} \right\rceil, \quad (6)$$

where δ is the length of the sub-slot. For synchronous MAC protocols, the synchronization accuracy should be in the granularity of δ .

The separate SPATIAL module simulates the mobility of the source nodes. The movement tracks of the source nodes are user-customized such that the simulator can cover many mobility models. The spatial simulator provides Application Programming Interfaces (APIs) for users to control the velocity and derivative of the velocity to implement highly complex mobility models. The spatial module uses a separated position-updating frequency from the MAC simulation, which accelerates the simulation of simple mobility models and further improves efficiency.

IV. EXPERIMENTS AND RESULTS

Four simulation experiments were designed to explore the impacts of source node distribution, propagation delay, transmission timing, mobility of source nodes, MAC configurations, and ML agents on the network performance. The source nodes were placed randomly within a sphere around the sink node with a radius of $L_{\text{max}} = 1500 \, \text{m}$, and the number of source nodes was $N \in [2,25] \cap \mathbb{Z}$. The experimental setups are shown in Table I.

Parameters common to all experiments were the maximum propagation delay, $\tau_{max} = 1$ s, and the simulation time per trial was 10 000 s. The transmission rate and packet

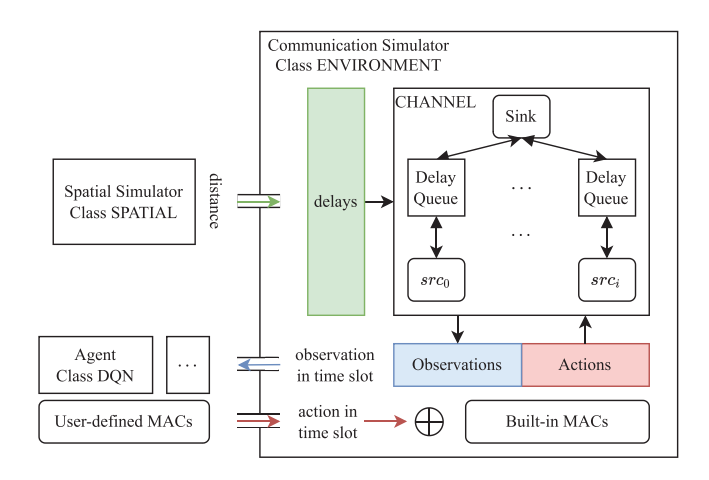


FIG. 3. (Color online) Structure of the simulator. The simulator consists of a communication simulator and a spatial simulator. The communication simulator uses three-level abstraction (ENVIRONMENT, CHANNEL, and DELAY_QUEUE) to achieve time-accurate simulation of MAC protocols, including user-defined protocols. The SPATIAL simulator simulates complex motions by providing second-order control APIs to the communication simulator.

length for each source node are set as constants of 5000 bps and 144 bits, respectively. Therefore, the packet duration $T_p=144/5000=0.0288\approx0.03\,\mathrm{s}$ (Geng and Zheng, 2022), guard time $T_g=0.03\,\mathrm{s}$, and simulation sub-slot length $\delta=0.01\,\mathrm{s}$. The maximum distance from source to sink is $L_{\mathrm{max}}=1500\,\mathrm{m}$, and the acoustic waveform propagation velocity is $V=1500\,\mathrm{m/s}$, therefore, the time slot length was set to $T=L_{\mathrm{max}}/V=1\,\mathrm{s}$ for synchronous networks and $T=0.2\,\mathrm{s}$ for asynchronous networks, except when exploring the effect of time slot length, and the time slot length was set from 0.1 to 1 s. All source nodes are saturated with packets to transmit, and the sink node can always accept the noncollided packets (Geng and Zheng, 2022).

The performance of the MAC protocols was measured by channel utilization with the unit of Erlang (Freeman, 2005; Park *et al.*, 2021). With a single sink node, the system channel utilization is the fractional amount of time that packets are successfully received at the sink node. Denoting the number of packets successfully received in time slot, t_0 , as $S(t_0)$, the channel utilization, $E(t_0)$, is calculated by

$$E(t_0) = S(t_0) \frac{T_p}{T}. (7)$$

In the experiments, we chose TDMA, ALOHA, and async-DL-MAC (Geng and Zheng, 2022) as examples of the contention-free protocols, the random access protocols, and the learning-based protocols, respectively. We thoroughly explored the impact of mobility on those protocols in our simulations using the lightweight simulator as well as NS-3 when possible, and the NS-3 results are similar to the self-made simulator's results.

A. Synchronous and asynchronous networks

The first experiment examined the static networks using the slotted ALOHA and TDMA MAC protocols. The slotted ALOHA is a random access MAC protocol in which each node independently decides to transmit a packet in a time slot with a probability, q. This experiment chose q=0.5 for synchronous ALOHA networks and asynchronous ALOHA networks. TDMA is a schedule-based MAC protocol that assigns exactly one node to one time slot in a round-robin fashion. Because the source nodes are randomly located in space and the propagation delays may be as large as $T-T_p$, TDMA in UAN can guarantee no collision by assigning one packet transmission in a time slot. TDMA groups N consecutive time slots as a time frame, where N is the number of source nodes in the

network. The synchronous trials followed the assumption that $T_r(n,t) \equiv 0 \quad \forall n \in [1,N] \cap \mathbb{Z} \quad \forall t \in \mathbb{Z}.$

Figure 4 compares the UAN synchronous and asynchronous MACs. T=1 s is chosen to guarantee collision-free for the TDMA and timing-correctness for synchronous ALOHA. On the other hand, the asynchronous ALOHA enabled concurrent transmission and used a shorter time slot, T=0.2 s, to increase channel utilization.

The TDMA used preassigned time slots to guarantee one transmission per time slot, resulting in a channel utilization as low as $1 \times 3/100 = 0.03$ regardless of the number of source nodes. Note that the TDMA UAN achieved a much lower channel utilization than that of RF TDMA networks, where the source nodes use $N \times T_p$ as a time frame without inserting large propagation delays between transmissions. In contrast, the synchronous ALOHA decided to transmit with a probability of q per time slot independently. If the synchronous ALOHA node decided to transmit in a time slot, it would transmit with a fixed start time. Therefore, the collision condition (3) depended on the random initial positions of the source nodes. The experiment ran 50 trials for every case of $N \in [2, 25] \cap \mathbb{Z}$. The averaged channel utilization over 50 trials illustrated a slow increase in channel utilization when the number of nodes, N, increases from 2 to 25.

Our experiment found that in UANs, the channel utilization of slotted ALOHA increased with N until reaching the maximum, 1/e (Sklar, 2021), at which point the network became saturated. Then, channel utilization decreased with N as the network became overloaded. Even if the asynchronous ALOHA node randomly picked the transmission interval, $T_r(n,t)$, the asynchronous ALOHA was still slotted ALOHA protocol because its transmission starting time was in a specific range inside the time slot and could only transmit one packet.

Our experiment also found that in synchronous ALOHA, as the number of nodes exceeds 25, the channel utilization continued to increase and reached a peak of 1/e when N=45 and then went down. This was not shown in Fig. 4. The asynchronous ALOHA used T=0.2 s, and its channel utilization reached its peak 1/e when the number of nodes was 12, and then the channel utilization gradually decreased as N>12. In essence, the theoretical maximum channel utilization, 1/e, could be achieved by the asynchronous ALOHA protocol with a smaller number of source nodes when T was smaller.

Figure 5 illustrates the detailed distribution of those 50 trials for synchronous ALOHA, where the right legend shows the maximum, minimum, 25th percentile (Q1),

TABLE I. Simulation setup for five experiments.

Experiment	1	2	3	4 Mobile	
Mobility	Static	Static and mobile	Mobile		
Network type	Synchronous or asynchronous	Asynchronous	Asynchronous	Asynchronous Yes	
ML agent	No	No	No		
MAC of non-agent	ALOHA and TDMA	ALOHA	ALOHA	Hybrid	

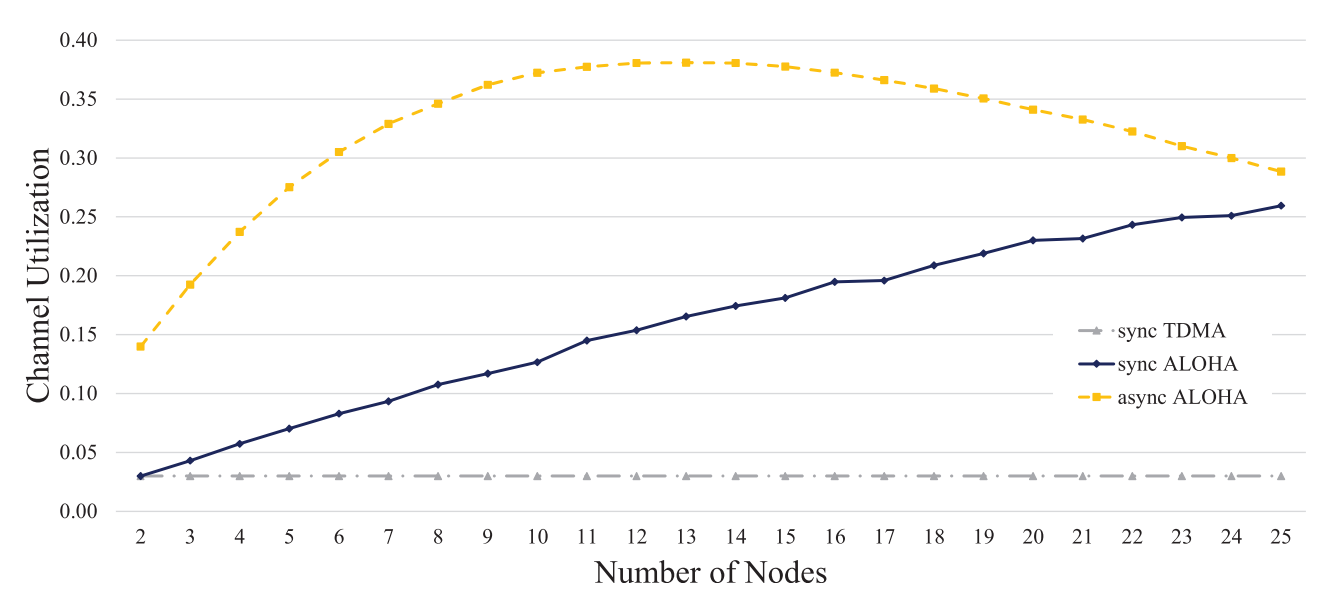


FIG. 4. (Color online) Channel utilization in synchronous or asynchronous networks.

median, and 75th percentile (Q3) of the channel utilization. The stars represent the mean channel utilization of the 50 trials, and the outliers are determined by $1.5 \times$ interquartile range (IQR), where IQR = Q3 - Q1. The upper and lower bounds were $Q3 + 1.5 \times IQR$ and $Q1 - 1.5 \times IQR$, respectively. The large variation of channel utilization was only exhibited in the synchronous ALOHA protocol because the impact of node positions was significant only in the synchronous network regarding packet collision. When any pair of nodes was located in a way that their propagation delays satisfied Eq. (3), collisions would always occur whenever the two nodes were transmitting signals in the same time slot, thus, severely reducing the channel utilization. This experiment demonstrated that the conventional RF synchronous MAC performed poorly when applied directly to UANs without concurrent transmission. In contrast, the asynchronous ALOHA enabled concurrent transmission and allowed the source node to delay a random time period,

 $T_r(n,t) \sim \mathcal{U}(0,T)$, if the node was to transmit signals in the time slot. The concurrent transmission employed the long propagation delay, and the random delay, $T_r(n,t)$, helped to avoid collisions caused by the initial positions of the source nodes. Therefore, the asynchronous ALOHA achieved saturation more easily and experienced low variations of channel utilization in the test trials, which was omitted in Fig. 4.

B. Static and mobile networks

The second experiment compared the difference in channel utilization between static and mobile networks when the source nodes were synchronous or asynchronous. This experiment used the slotted ALOHA with q = 0.5, and different trials used the same initial positions to eliminate the variation introduced by location initialization as discussed in Sec. IV A. The mobile trials used the AUVassisted and moored floating sensor models, which were introduced in Sec. III, to represent high- and low-velocity

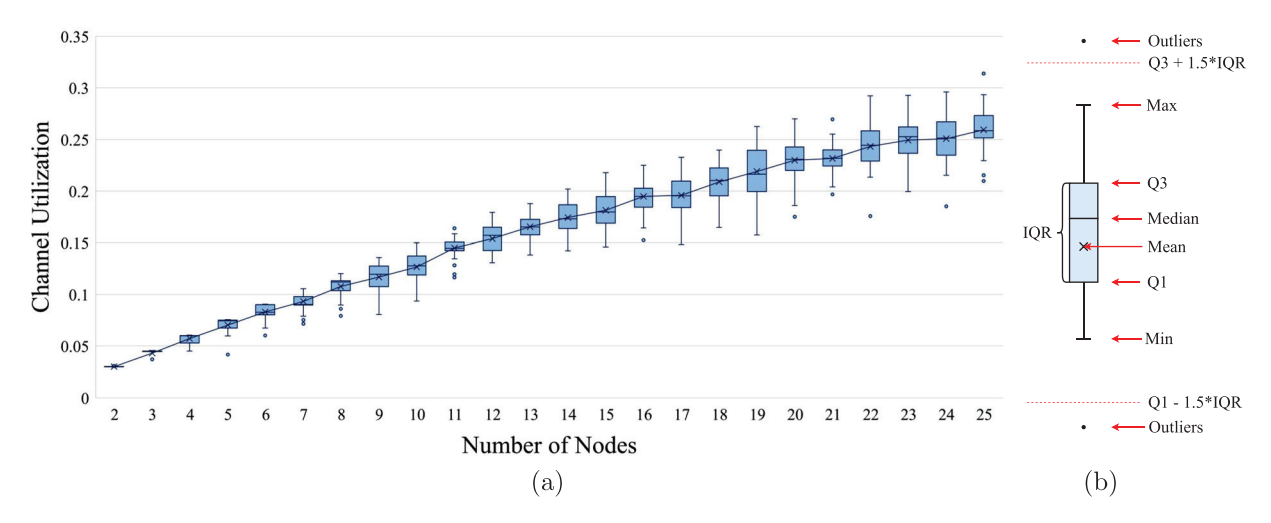


FIG. 5. (Color online) Performance of static synchronous ALOHA networks depends significantly on the placement of the source nodes.

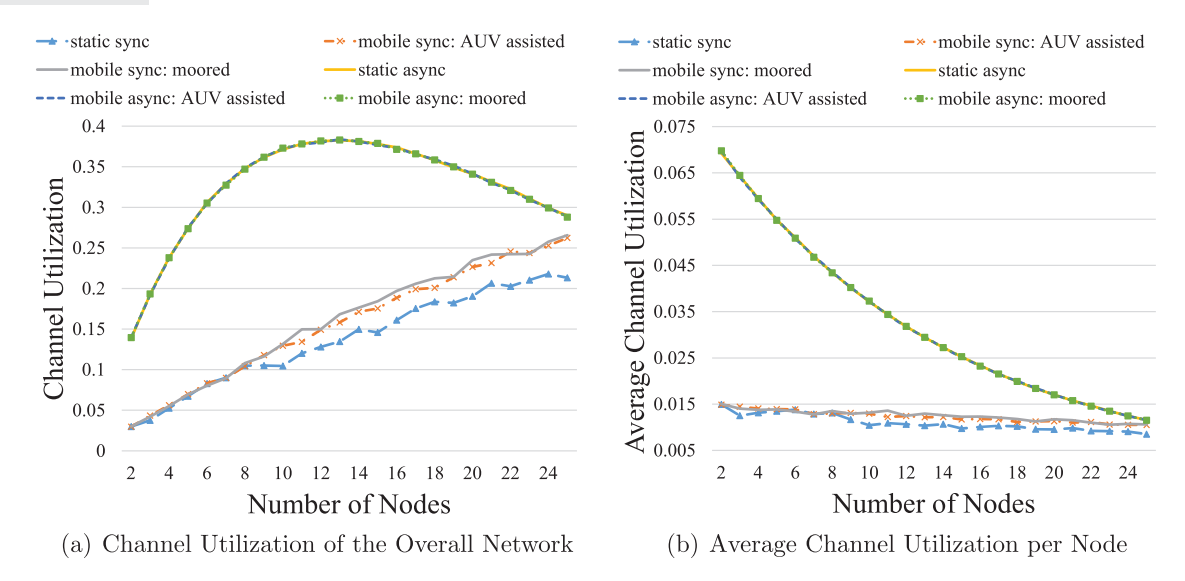


FIG. 6. (Color online) Channel utilization of static and mobile ALOHA networks with q = 0.5.

scenarios. The high mobility led to large variations in propagation delays on the order of $0.01\,\mathrm{s}$. Figure 6 illustrates the channel utilization of randomly initialized nodes under static or mobile, synchronous or asynchronous networks, where Fig. 6(a) shows channel utilization of the overall network and Fig. 6(b) shows the average channel utilization per node.

The asynchronous ALOHA networks, either static or mobile, achieved very similar performances in channel utilization, as their average curves nearly overlapped. On the other hand, mobility in synchronous ALOHA slightly enhanced the mean channel utilization over the static synchronous ALOHA. The 50 trials in the experiment also showed less variation of channel utilization in mobile synchronous ALOHA than in static synchronous ALOHA. This was because mobility introduced varying propagation delays that were similar to the initial delays of the asynchronous network. Therefore, the mobile synchronous network achieved higher channel utilization than the static, given the same MAC protocols. The tendency was clearer when N > 20, and the maximum performance appeared when N = 25, at which the mobile moored network achieved 23% higher channel utilization than the static network. Compared with two different mobile models, we found that the lowvelocity model (moored) achieved slightly higher channel utilization than the high-velocity model (AUV-assisted) did.

Although the overall network channel utilization fluctuated according to the number of source nodes, N, the average channel utilization per node decreased monotonically with the number of nodes in synchronous and asynchronous ALOHA protocols and mobile and static networks, as depicted in Fig. 6(b).

C. Mobile system exploration

The third experiment examined the parameter combination in mobile asynchronous ALOHA networks. Figure 7 illustrates the channel utilization under different transmission probabilities, q, and different time slot lengths, T. The general patterns indicated that the network load increased as the number of nodes increased.

The ALOHA transmission probability, q, was negatively correlated to the number of source nodes at the saturation point. To reach the saturated channel utilization, as the transmission probability of each node, q, changed from 0.1 to 0.9, the saturation point was shifted left, as displayed in Fig. 7(a). The numbers of nodes that achieved saturation were 36, 28, 21, 16, 13, 11, 9, 8, and 7. Therefore, the transmission probability, q, should be chosen according to the number of nodes in the network. Especially when deploying new sensors in a well-tuned ALOHA Wireless Sensor Network (WSN), a smaller q would be better than keeping the original one.

The packet-to-time slot ratio, $T_p:T$, was positively correlated to the number of source nodes at the network's saturation point. When the time slot length, T, changed from 0.1 to 1 s, the saturation point was shifted right, as shown in Fig. 7(b). In this experiment, the packet duration was fixed, $T_p=0.03$ s, and the ratio, $T_p:T$, in the legends represented the length of time slot, T, as it changed from 0.1 to 1 s. The results exhibited that for a small-scale WSN, where $N \leq 6$, a small length of time slot, $T \leq 0.3$ s, could use communication resources efficiently. For a medium-scale WSN, where $N \in [7,20]$, the $T \in [0.3,0.4]$ s provided good channel utilization. As for a large-scale WSN, where $N \geq 21$, only the $T \geq 0.5$ s could satisfy such heavy concurrent transmission.

D. Al-agent node in mobile networks

The fourth experiment evaluated the impact of an AI-agent node on static and mobile networks. To enable learning in the AI node, a downlink from the sink node to all sources was added to the communication model in Sec. III. At the end of every time slot, the sink node broadcasts its status as feedback in the format {0,1,2}, representing collision, idle, and success, respectively. The feedback of sink status to all nodes used a different frequency channel to

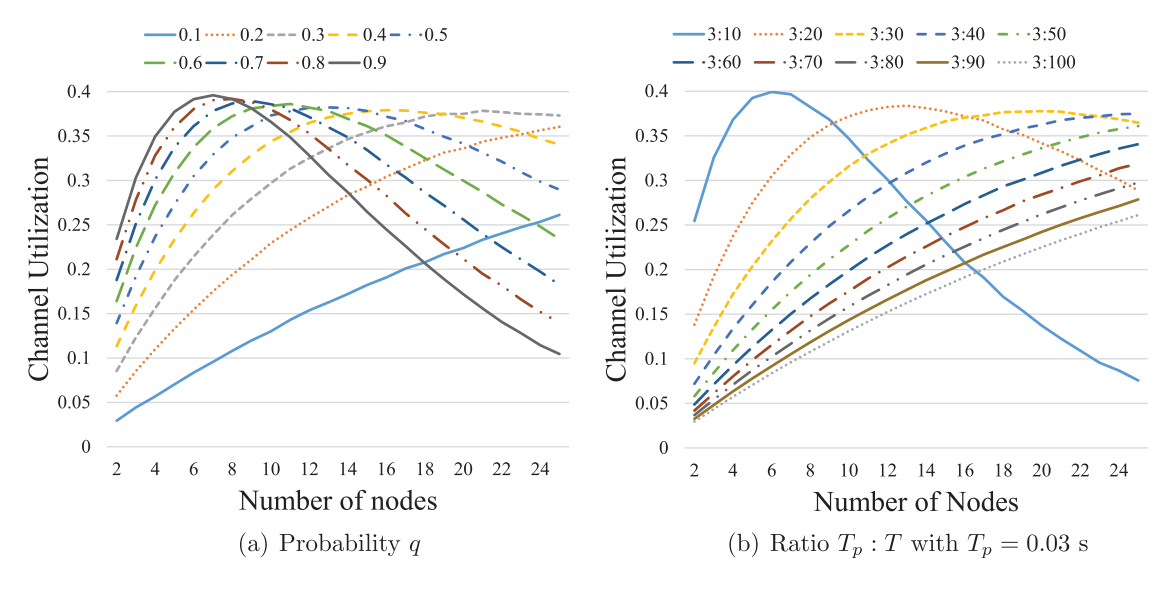


FIG. 7. (Color online) Channel utilization in mobile asynchronous ALOHA network with different configurations.

avoid overlapping between the downlink and uplink. The propagation delay of the feedback link is also included in the simulation. This experiment tested six different setups of coexisting networks that represented different scenarios, as displayed in Table II.

The (N-1) non-agent nodes in the network used ALOHA with a transmission probability, q=0.5. Because they were distributed at different positions, all source nodes would receive the feedback signal at different delays. The agent used the feedback signals and their time stamps from the sink to observe the network behavior, constructed a state from observations of several time slots, and learned to take actions to use idle time slots in the network (Geng and Zheng, 2022; Yu *et al.*, 2019).

The AI-agent node used the async-DL-MAC algorithm to learn the environment and use the time gaps for transmission (Geng and Zheng, 2022; Yu et al., 2019). The instantaneous network state at t, denoted as $s_t = \{a_t, obs_t, R_t\}$, was a combination of the past actions, a_t , observations, obs_t, and previous rewards, R_t . The input of the deep Q-learning network (DQN), $S_t = \{s_{t-1}, s_{t-2}, ..., s_{t-M}\}$, was the combination of several consecutive past instantaneous states, and the state length was M = 20 time slots in this experiment. In addition, the model kept a memory with long-term past states and randomly picked some past states to train the model to avoid being trapped by local optima. The memory size was selected as 1000 past states in this experiment. The action was taken as follows:

$$a_t = \arg_a \max Q(\mathbf{S}_t, \mathbf{A}),\tag{8}$$

where Q was the Q-value or output of the neural network, and A was the collection of all possible actions. In the synchronous mode, the agent chose $\{0,1\}$, which corresponded to staying idle or transmitting. In the asynchronous mode, the agent took actions, $\{0,1,2,...,K\}$, which corresponded to staying idle or transmitting with $T_r(n,t)=0,1,2,...,K-1$. The observations took values as $\{SUCCESS, IDLE, COLLISION\}$, and

the rewards for these observations were set as $\{1,0,-1\}$, respectively.

The training of neural networks required a target value as the ground truth to calculate the loss. Neural networks used the loss to apply the backpropagation algorithm to calculate gradients of parameters to the target value. The neural network then applied stochastic gradient descent (SGD) with learning rate, $\eta=0.01$, to update parameters. The target value used for neural network training was calculated by the Bellman equation as

$$\begin{aligned} \text{DQN}(S_t) &\approx Q(S_t, A), \ Q_{\text{target}}(S_t, a_t) \\ &= (1 - \alpha)Q(S_t, a_t) \\ &+ \alpha (R_t + \gamma \max Q(S_t', a_t)), \end{aligned} \tag{9}$$

where $\gamma=0.9$ is the learning discount factor and $\alpha=1$ is the Q-learning rate. The Q-learning also applied ϵ -greedy to have a balance between exploration and exploitation, where the epsilon greedy factor was $\epsilon=\min\{0.01,1\times(0.995)^i\}$, where i is the number of iterations.

The neural network used in this experiment had 8 fully connected hidden layers with 64 neurons in each hidden layer and used rectified linear unit (Goodfellow *et al.*, 2016) as an activation function. In addition, three shortcut connections were added to construct ResNet blocks (He *et al.*, 2016) in the neural network. The number of parameters of the neural network was on the order of 54 000 = 54K, which was rather lightweight in comparison to existing deep learning models. To further reduce computational complexity, the training process was applied with a period of 5 time slots, and the input was grouped with a batch size of 64.

Under the static network scenarios of setups 1–3, the asynchronous agent significantly improved the channel utilization when $N \le 14$. By comparing results under setup 1 and setup 2 in Fig. 8(a), a higher channel utilization was observed with an asynchronous agent when $N \le 14$ and a synchronous agent when N > 14. The asynchronous agent



TABLE II. Simulation setups for the experiment with an agent node and (N-1) non-agent nodes.

Setup number	1	2	3	4	5	6
Agent MAC Mode Non-agent MAC mode	Asynchronous	Synchronous	Asynchronous	Asynchronous	Asynchronous	Asynchronous
	Synchronous	Synchronous	Asynchronous	Asynchronous	Asynchronous	Asynchronous
Agent mobility Non-agent mobility	Static	Static	Static	Mobile	Static	Mobile
	Static	Static	Static	Static	Mobile	Mobile

learned from the environment and effectively used the idle sub-slot to increase the channel utilization with fewer users in an unsaturated channel. Still, the agent experienced difficulties in learning ALOHA-based MAC networks with more users in a saturated channel. By comparing setup 3 results in Fig. 8(a) and the async ALOHA curve in Fig. 4, it was clear that the network with an asynchronous agent outperformed the network without agents when $N \leq 14$. However, the existence of agents increased the overall network load, and the channel utilization reached saturation with an N smaller than that of non-agent networks. Therefore, the system showed lower performance when N > 14. Furthermore, the maximum channel utilization was around 1/e because of ALOHA nodes. The synchronous agent network's channel utilization was similar to that of pure ALOHA networks because employing the long propagation delays was difficult for synchronous agents, which had only limited actions to take. In setups 1 and 2, the channel utilization curves were the results of a single trial with random initial locations of the nodes. The dip at N = 12 displayed high potential collisions and reduced channel utilization resulting from some pairs of randomly initialized nodes located from similar distances to the sink node. Overall, the agent node was able to significantly improve channel utilization of static networks, as shown in Fig. 8(b), when the agent has sufficient flexibility to determine transmission time.

Under mobile network scenarios with setups 4–6, the asynchronous agent significantly improved the network throughput and overall channel utilization when the total number of nodes

was less than 14, as shown in Figs. 8(b) and 8(a). The overall channel utilization slowly degraded when N exceeded 14 and so did the agent's contribution due to the saturation of the network when too many nodes competed for the channel. The performance of setups 4-6 was similar to that of setup 3, regardless of the mobility of the nodes. Furthermore, the channel utilization curves of setups 3-6 reassembled the shape of those in pure asynchronous static networks shown in Figs. 7(a) and 6(b). Combining the curves of setups 3-6 in Fig. 8(a), q = 0.5 in Fig. 7(a), and $T_p : T = 3 : 20$ in Fig. 6(b), the network with agent nodes of setups 3-6 reached saturation when N = 12, whereas the networks without agents reached saturation at N = 14. The reason was that the agent used a channel with wider bandwidth than a q = 0.5 ALOHA node did when the overall channel was unsaturated. However, when the channel reached saturation with N > 14, the agent still occupied more channel bandwidth than an average non-agent node.

Comparing all six setups in experiment 4, it could be concluded that with the mobility of nodes in the network, it was difficult for the agent to learn the channel or use the available bandwidth and empty time slots. It could also be decided that asynchronous transmission in all nodes would significantly enhance the channel utilization over synchronous networks, especially when the total number of nodes was small.

V. CONCLUSION

This paper has investigated a wide range of MAC protocols for underwater acoustic networks in which a large

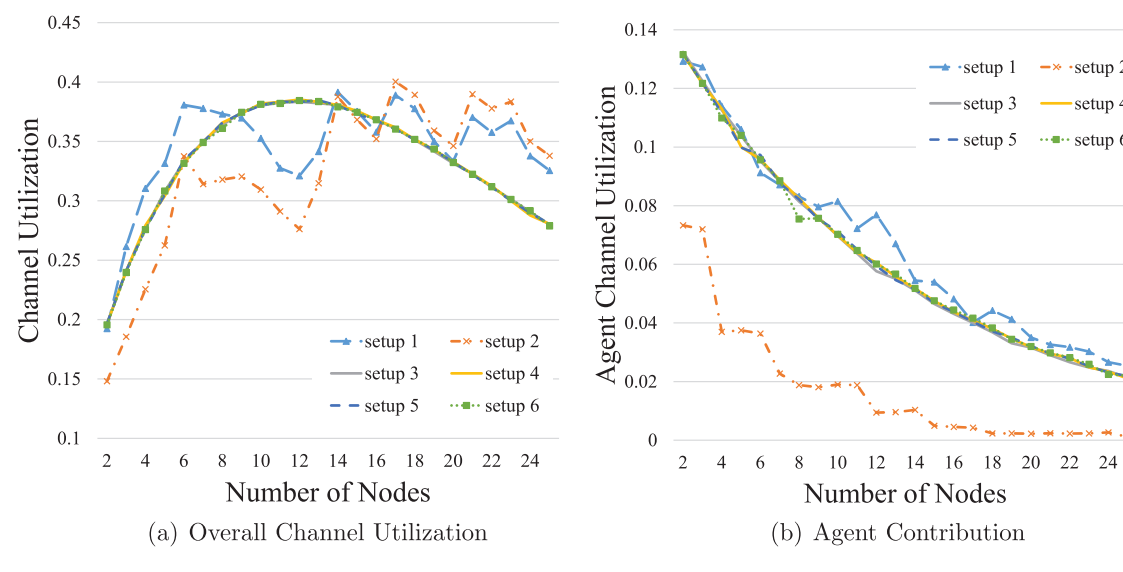


FIG. 8. (Color online) Networks with one agent node and (N-1) ALOHA nodes and q=0.5.

https://doi.org/10.1121/10.0026232

number of source nodes transmit packets to a single sink node. A lightweight MAC simulator and NS-3 have been used to accurately model the propagation delay and timing of underwater mobile acoustic networks. Four sophisticated experiments have been conducted to simulate static and/or mobile, synchronous and/or asynchronous protocols, with or without the AI-agent node. The channel utilization results show that the asynchronous protocols outperform synchronous protocols as the asynchronous networks achieve a higher packet duration to slot-length ratio. The mobile nodes in a synchronous network would enhance channel utilization as mobility adds timing variations in transmission, which is similar to the effect of asynchronous protocols. In contrast, adding node mobility to asynchronous protocols has less improvement in channel utilization than adding mobility to synchronous protocols. Adding an AI agent in either synchronous or asynchronous protocols significantly improves the network throughput and channel utilization when the number of source nodes is small and the channel is unsaturated. AI-agent nodes in mobile asynchronous networks experience difficulties in learning the channel conditions or using the channel resources.

AUTHOR DECLARATIONS Conflict of Interest

The authors have no conflicts to disclose.

DATA AVAILABILITY

The data that support the findings of this study are available from the corresponding author upon reasonable request. The data that support the findings of this study are generated by a self-made lightweight simulator and NS-3 (Riley and Henderson, 2010; UAN, 2024). The lightweight simulator is open-sourced and can be accessed at https:// github.com/ruoyuwang79/HMMACS. The NS-3 script used in this study is also provided in the repository. The NS-3 is openly available in https://www.nsnam.org/ at https://dl.acm. org/doi/10.1145/1096166.1096174. All experiment results can be reproduced by using the provided repository.

- Akyildiz, I. F., Pompili, D., and Melodia, T. (2005). "Underwater acoustic sensor networks: Research challenges," Ad hoc Networks 3(3), 257–279.
- Akyildiz, I. F., Wang, P., and Sun, Z. (2015). "Realizing underwater communication through magnetic induction," IEEE Commun. Mag. 53(11), 42 - 48
- Alfouzan, F. A., Shahrabi, A., Ghoreyshi, S. M., and Boutaleb, T. (2019). "A collision-free graph coloring MAC protocol for underwater sensor networks," IEEE Access 7, 39862-39878.
- Al Guqhaiman, A., Akanbi, O., Aljaedi, A., and Chow, C. E. (2021). "A survey on MAC protocol approaches for underwater wireless sensor networks," IEEE Sens. J. 21(3), 3916-3932.
- Assaf, T., Stefanini, C., and Dario, P. (2013). "Autonomous underwater biorobots: A wireless system for power transfer," IEEE Robot. Automat. Mag. 20(3), 26-32.
- Beerens, S., Ridderinkhof, H., and Zimmerman, J. (1994). "An analytical study of chaotic stirring in tidal areas," Chaos, Solitons Fractals 4(6),
- Campagnaro, F., Francescon, R., Guerra, F., Favaro, F., Casari, P., Diamant, R., and Zorzi, M. (2016). "The DESERT underwater framework v2: Improved capabilities and extension tools," in 2016 IEEE Third

- Underwater Communications and Networking Conference (UComms), Lerici, Italy (August 30-September 1, 2016) (IEEE, New York), pp. 1-5.
- Caruso, A., Paparella, F., Vieira, L. F. M., Erol, M., and Gerla, M. (2008). "The meandering current mobility model and its impact on underwater mobile sensor networks," in IEEE INFOCOM 2008-The 27th Conference on Computer Communications, Phoenix, AZ (April 13-18, 2008) (IEEE, New York), pp. 221-225.
- Chen, W., Guan, Q., Yu, H., Ji, F., and Chen, F. (2021). "Medium access control under space-time coupling in underwater acoustic networks," IEEE Internet Things J. 8(15), 12398-12409.
- Chirdchoo, N., Soh, W.-S., and Chua, K. C. (2007). "Aloha-based MAC protocols with collision avoidance for underwater acoustic networks," in IEEE INFOCOM 2007—26th IEEE International Conference on Computer Communications, Anchorage, AK (May 6-12, 2007) (IEEE, New York), pp. 2271-2275.
- Chitre, M., Bhatnagar, R., and Soh, W.-S. (2014). "UnetStack: An agentbased software stack and simulator for underwater networks," in 2014 Oceans-St. John's, St. John's, NL, Canada (September 14-19, 2014) (IEEE, New York), pp. 1-10.
- Chitre, M., and Soh, W. S. (2015). "Reliable point-to-point underwater acoustic data transfer: To juggle or not to juggle?," IEEE J. Ocean. Eng. 40(1), 93-103.
- Chu, Y., Mitchell, P. D., and Grace, D. (2012). "ALOHA and Q-learning based medium access control for wireless sensor networks," in 2012 International Symposium on Wireless Communication Systems (ISWCS), Paris France (August 28-31, 2012) (IEEE, New York), pp. 511-515.
- Diamant, R., Campagnaro, F., De Grazia, M. D. F., Casari, P., Testolin, A., Calzado, V. S., and Zorzi, M. (2017). "On the relationship between the underwater acoustic and optical channels," IEEE Trans. Wireless Commun. 16(12), 8037-8051.
- Fang, D., Li, Y., Huang, H., and Yin, L. (2010). "A CSMA/CA-based MAC protocol for underwater acoustic networks," in 2010 6th International Conference on Wireless Communications Networking and Mobile Computing (WiCOM), Chengdu, China (September 23-25, 2010) (IEEE, New York), pp. 1-4.
- Freeman, R. L. (2005). Fundamentals of Telecommunications (Wiley, Hoboken, NJ).
- Geng, X., and Zheng, Y. R. (2022). "Exploiting propagation delay in underwater acoustic communication networks via deep reinforcement learning," IEEE Trans. Neural Networks Learn. Syst. 34(12), 10626-10637.
- Goodfellow, I., Bengio, Y., and Courville, A. (2016). Deep Learning (MIT Press, Cambridge, MA).
- Han, S., Noh, Y., Lee, U., and Gerla, M. (2013). "M-FAMA: A multisession MAC protocol for reliable underwater acoustic streams," in 2013 Proceedings IEEE INFOCOM, Turin, Italy (April 14-19, 2013) (IEEE, New York), pp. 665-673.
- Han, Y., and Fei, Y. (2016). "DAP-MAC: A delay-aware probability-based MAC protocol for underwater acoustic sensor networks," Ad Hoc Networks 48, 80-92.
- He, K., Zhang, X., Ren, S., and Sun, J. (2016). "Deep residual learning for image recognition," in Proceedings of the IEEE Conference on Computer Vision and Pattern Recognition, Las Vegas, NV (June 26-July 1, 2016) (IEEE, New York), pp. 770-778.
- Hwang, H. Y., and Cho, H.-S. (2016). "Throughput and delay analysis of an underwater CSMA/CA protocol with multi-RTS and multi-DATA receptions," Int. J. Distrib. Sensor Networks 12(5), 1-9.
- Jiang, S. (2017). "State-of-the-art medium access control (MAC) protocols for underwater acoustic networks: A survey based on a MAC reference model," IEEE Commun. Surv. Tutorials 20(1), 96-131.
- Kredo, K., II, Djukic, P., and Mohapatra, P. (2009). "Stump: Exploiting position diversity in the staggered TDMA underwater MAC protocol," in IEEE INFOCOM 2009, Rio de Janeiro, Brazil (April 19-25, 2009) (IEEE, New York), pp. 2961-2965.
- Lee, C., and Bogue, N. M. (2011). "Advanced development associated with the glider technology transition initiative," Technical Report, Washington University Seattle Applied Physics Lab.
- Li, Z., Guo, Z., Qu, H., Hong, F., Chen, P., and Yang, M. (2009). "UD-TDMA: A distributed TDMA protocol for underwater acoustic sensor network," in 2009 IEEE 6th International Conference on Mobile Ad hoc and Sensor Systems, Macau (October 12-15, 2009) (IEEE, New York), pp. 918-923.

JASA

https://doi.org/10.1121/10.0026232

- Lmai, S., Chitre, M., Laot, C., and Houcke, S. (2017). "Throughput-efficient super-TDMA MAC transmission schedules in ad hoc linear underwater acoustic networks," IEEE J. Ocean. Eng. 42(1), 156–174.
- Morozs, N., Mitchell, P., and Zakharov, Y. V. (2018). "TDA-MAC: TDMA without clock synchronization in underwater acoustic networks," IEEE Access 6, 1091–1108.
- Nguyen, H. T., Shin, S.-Y., and Park, S.-H. (2007). "State-of-the-art in MAC protocols for underwater acoustics sensor networks," in *International Conference on Embedded and Ubiquitous Computing*, Taipei, Taiwan (December 1–4, 2017) (Springer, Berlin, Heidelberg), pp. 482–493.
- Park, S. H., Mitchell, P. D., and Grace, D. (2019). "Reinforcement learning based MAC protocol (UW-ALOHA-Q) for underwater acoustic sensor networks," IEEE Access 7, 165531–165542.
- Park, S. H., Mitchell, P. D., and Grace, D. (2021). "Reinforcement learning based MAC protocol (UW-ALOHA-QM) for mobile underwater acoustic sensor networks," IEEE Access 9, 5906–5919.
- Parrish, N., Tracy, L., Roy, S., Arabshahi, P., and Fox, W. L. (2008). "System design considerations for undersea networks: Link and multiple access protocols," IEEE J. Select. Areas Commun. 26(9), 1720–1730.
- Peleato, B., and Stojanovic, M. (2007). "Distance aware collision avoidance protocol for ad-hoc underwater acoustic sensor networks," IEEE Commun. Lett. 11(12), 1025–1027.
- Petrioli, C., Petroccia, R., Potter, J. R., and Spaccini, D. (2015). "The sunset framework for simulation, emulation and at-sea testing of underwater wireless sensor networks," Ad Hoc Networks 34, 224–238.
- Pompili, D., Melodia, T., and Akyildiz, I. F. (2007). "A distributed CDMA medium access control for underwater acoustic sensor networks," in *Proceedings of the Mediterranean Ad Hoc Networking Workshop* (Citeseer, Princeton, NJ).
- Purcell, M., Gallo, D., Packard, G., Dennett, M., Rothenbeck, M., Sherrell, A., and Pascaud, S. (2011). "Use of REMUS 6000 AUVs in the search for the air France flight 447," in *OCEANS'11 MTS/IEEE KONA*, Waikoloa, HI (September 19–22, 2011) (IEEE, New York), pp. 1–7.
- Rahman, P., Karmaker, A., Alam, M. S., Hoque, M. A., and Lambert, W. L. (2019). "CUMAC-CAM: A channel allocation aware MAC protocol for addressing triple hidden terminal problems in multi-channel UWSNs," SN Appl. Sci. 1, 1–20.

- Riley, G. F., and Henderson, T. R. (2010). "The NS-3 network simulator," in *Modeling and Tools for Network Simulation* (Springer, Berlin, Heidelberg), pp. 15–34.
- Shepard, C., Yu, H., Anand, N., Li, E., Marzetta, T., Yang, R., and Zhong, L. (2012). "Argos: Practical many-antenna base stations," in *Proceedings of the 18th Annual International Conference on Mobile Computing and Networking*, Istanbul, Turkey (August 22–26, 2012) (ACM, New York), pp. 53–64.
- Sitanayah, L., Sreenan, C. J., and Brown, K. N. (2010). "ER-MAC: A hybrid MAC protocol for emergency response wireless sensor networks," in 2010 Fourth International Conference on Sensor Technologies and Applications, Venice, Italy (July 18–25, 2010) (IEEE, New York), pp. 244–249.
- Sklar, B. (2021). Digital Communications: Fundamentals and Applications (Prentice Hall, Upper Saddle River, NJ).
- Stojanovic, M., and Preisig, J. (2009). "Underwater acoustic communication channels: Propagation models and statistical characterization," IEEE Commun. Mag. 47(1), 84–89.
- UAN (2024). "Network simulator 3 UAN framework," available at https://www.nsnam.org/docs/models/html/uan.html (Last viewed June 5, 2024).
- Williamson, B. J., Fraser, S., Blondel, P., Bell, P. S., Waggitt, J. J., and Scott, B. E. (2017). "Multisensor acoustic tracking of fish and seabird behavior around tidal turbine structures in Scotland," IEEE J. Ocean. Eng. 42(4), 948–965.
- Yu, Y., Wang, T., and Liew, S. C. (2019). "Deep-reinforcement learning multiple access for heterogeneous wireless networks," IEEE J. Select. Areas Commun. 37(6), 1277–1290.
- Zeng, H., Hou, Y. T., Shi, Y., Lou, W., Kompella, S., and Midkiff, S. F. (2017). "A distributed scheduling algorithm for underwater acoustic networks with large propagation delays," IEEE Trans. Commun. 65(3), 1131–1145.
- Zheng, Y. R., Wu, J., and Xiao, C. (2015). "Turbo equalization for single-carrier underwater acoustic communications," IEEE Commun. Mag. 53(11), 79–87.
- Zhuo, X., Yang, H., Liu, M., Wei, Y., Yu, G., and Qu, F. (2022). "Data concurrent transmission MAC protocol for application oriented underwater acoustic sensor networks," China Commun. 19(10), 220–237.